RSC Advances

ROYAL SOCIETY OF CHEMISTRY

www.rsc.org/advances

Chemisorbed oxygen atom on the activation of C-H bond in methane: A Rh model study

Ying-Qi Wang [1], Cun-Qin Lv [2,*] and Gui-Chang Wang [3,4,*]

([1] School of Chemistry and Chemical Engineering, Shandong University, Jinan, 250100, P.R.China; [2] College of Chemistry and Enviromental Engineering, Shanxi Datong University, Datong 037009, Shanxi Province, P. R. China; [3] Department of Chemistry,Nankai University, Tianjin 300071, P. R. China; [4] State Key Laboratory of Coal Conversion, Institute of Coal Chemistry, Chinese Academy of Sciences, Taiyuan, 030001, P. R. China)

[*]Author to whom correspondence should be addressed.

Electronic mail: wangguichang@nankai.edu.cn; lcq173@126.com

Abstract: Single atom catalysts usually show unique catalytic activity and the physical nature is not clear. In the present work, density functional theory calculations are presented for adsorption and dissociation of CH_4 on clean and oxygen atom pre-adsorbed Rh metal surfaces with different coordinate number such as (111), (100), (110), (211), kink, ad-row (add two atom on a p(2x2)-111 unit cell) and ad-atom (add one atom on a p(2x2)-111 unit cell). The present calculation results show that the pre-adsorbed oxygen atom inhibits the methane dehydrogenation on Rh surfaces in general except on ad-atom model where it has no effect, and thus the possibility of the partial oxidation of methane to produce syngas (the mixture of CO and H_2) on Rh ad-atom catalysts. Having been analyzed by the barrier decomposition method, it was found that the presence of oxygen atom usually reduces the adsorption energy of dissociated fragments and increases the interaction between the dissociated fragments, both of which lead to an increase of the reaction barrier. Moreover, the electronic analysis indicated that the oxygen effect can be attributed to the strong interaction of acid-base pair sites on oxygen-metal systems, and a strong acid-base interaction related to the low dehydrogenation barrier.

Keywords: Methane; C-H bond activation; Oxygen species; Rh model catalysts; Density functional calculations.

1. Introductions

It is important to control bond break/formation in chemical processes, and high selectivity is required for a given catalytic reaction.[1-11] The catalytic reactivity and selectivity of surfaces are found to be dominated by low-coordinated atoms such as step-edge sites, and research showed that the step Ni(211) is favorable for C-C bond breaking rather than C-H bond breaking, while opposite trend occurs over flat Ni(111), and the reactivity of Ni(211) can be altered by the addition of Ag atom.[11]

It is well-known that methane is a low-cost material which could provide energy by hydrogen extraction. Usually transition metals like Pt, Pd and Rh are regarded as effective catalysts in methane dehydrogenation processes to produce H_2, particularly for the partial oxidation to form syngas (a $CO+H_2$ mixture), and thus have been extensively investigated from experimental and theoretical aspects. [12-40] Most recently, single-atom catalysts (SAC) have attracted much attention due to their unique catalytic properties and potential utility in heterogeneous catalysis including oxidation, water gas shift and hydrogenation.[41] Through theoretical study, it was found that the energy barrier of methane dehydrogenation over MoO_3-(010) supported isolated Pt ad-atom surface is far lower than that of flat Pt(111) surface, whereas the further dehydrogenation of methyl is limited.[38] Similarly, study about methane dehydrogenation on a series of Rh model catalysts found that although the first dehydrogenation of methane is significantly promoted, methyl dehydrogenation is inhibited on the Rh ad-atom model(i.e., a single atom catalyst model),[30] which is because the formed methylene radical has to form two bonds with substrates and such requirement cannot be met on isolated ad-atom easily. Recently theoretical study about methane oxidation on isolated ionic Pt atom-doped CeO_2 found that the reactivity of methane oxidation increases with the increase of the amount of isolated ionic Pt atom on CeO_2 support, which is due to the reason that the presence of Pt weakens the bond between the oxygen atoms located in its neighborhood and therefore activates them.[35] However, their study focused on the initial oxidation step, namely from methane to methyl, and ignored the further step.

It is well-known that the catalytic activity of X-H (X = C, H, O, N, or S) bond scission would significantly altered by oxygen atom since the strong O-H bond formed. Interestingly, both the experimental and theoretical studies demonstrated that the effect of chemisorbed oxygen atoms on the activation of X–H bonds scission depends strongly on the nature of the metals, namely, facilitating the X-H bond scission on less reactive metals like IB groups, and inhibiting the X-H bond cleavage on reactive metals like Ni and Fe/W. [42-47] For the oxidative dehydrogenation (ODH) of CH_4 via adsorbed

oxygen atom (O_{ad}) on Pd_{210} cluster, theoretical study[36] found that the reaction barrier is significantly larger than that of the pyrolytic dehydrogenation (i.e. direct dehydrogenation reaction) due to the larger repulsive interaction between the adsorbed O_{ad} and H-atom in CH_x species at transition sate. Moreover, it was found that on both clean and O_{ad} pre-adsorbed Pt surfaces the barrier decreases with the decrease of the coordination number(CN) of surface atom.[35] Similar result was also reported in the study of ODH of CH_x by O_{ad} on Pt(111) and Pt(211).[36]

Considering that catalytic activity can be significantly altered by the co-adsorbed species like oxygen atom, and the single Rh ad-atom model catalyst inhibits the methyl dehydrogenation due to the insufficient active site available, [30,38] one may expect if one or more oxygen species were introduced into the Rh added-tom system, the co-adsorbed oxygen species may act as an extra 'active site', namely Rh and O atoms simultaneously interact with methyl and may assist the dehydrogenation process. Inspired by such point, the methane dehydrogenation on a series of Rh model catalysts with and without co-adsorbed oxygen atom was systematically studied by the first principles density functional calculations, focusing on the relation between dehydrogenation activity and the CN of the active metal site as well as the effect of co-adsorbed oxygen species.

2. Calculation method and models

To investigate the energy and structural details of methane dissociation on Rh surfaces, we did periodic, self-consistent DFT calculations that were performed with VASP (Vienna ab initio simulation package).[48-50] The exchange-correlation effects have been described within the generalized gradient approximation (GGA), with the use of the Perdew–Wang (PW91) functional.[51] The electron-core interaction was described with the projector-augmented plane-wave (PAW) method.[52,53] All calculations were performed with a cutoff energy of 400 eV. The Brillouin zone was sampled with the Monkhorst-Pack grid.[54] Electronic energies were calculated with a (3×3×1) Monkhorst-Pack mesh k-points. The flat (111), (100) and (110) surfaces were modeled by a p(2x2) unit cell containing four layers that were separated by a 15 Å vacuum. During the optimization the adsorbates and the top two layers were relaxed and the bottom two layers were fixed at the bulk-truncated positions with the theoretical lattice constant of 3.86 Å. The add-row (add-atom) models were modeled by adding two (one) extra Rh atoms onto fcc site of (111) slab model per supercell. Therefore the supercells of (111), ad-atom and ad-row contain 16, 17 and 18 atoms, respectively. The ad-atom model was used to simulate the single atom site catalysts.[41] The Rh(211) slab

composed of twelve layers, including total 24 Rh atoms in the p(2x1) supercell, and the top six layers were relaxed during the optimization. The kinked surfaces were constructed by removing one edge atom at the step in a (1x3) unit cell of the (211) surface. The CN of the surface atom is 9, 8, 7, 7, 6, 5 and 3 for (111), (100), (110) (211), kink, ad-row, and ad-atom, respectively. The possible adsorption sites of these models are shown in Figure 1. The climbing-nudged elastic band method (cNEB) was employed to locate transition states (TSs).[55] In addition, the frequency analysis was performed to confirm the transition state. Vibrational frequencies were calculated by a second order finite difference approach with a step size of 0.015 Å. In this work, the adsorption energy ($\boldsymbol{E}_{ads}$) and the activation energy ($\boldsymbol{E}_a$) were calculated by the following two formulas: $\boldsymbol{E}_{ads} = E_{A/M} - E_M - E_A$ and $\boldsymbol{E}_a = E_{TS} - E_{IS}$, Here, $E_{A/M}$, E_M, E_A, E_{TS} and E_{IS} mean the calculated energies of the adsorption system, substrate, adsorbate, transition state (TS) and initial state (IS), respectively.

3. Results and discussion

3.1 Adsorption energy trends of possible species

In order to find out how CH_4 dissociation is affected by the existence of an oxygen atom, the first two dehydrogenation/oxidative dehydrogenation steps ($CH_4 \rightarrow CH_3+H$ and $CH_3 \rightarrow CH_2+H$) were studied in the present work. First we investigated the adsorption energies and configurations of possible species involved in the processes of methane dehydrogenation/oxidative dehydrogenation (see Tables 1, 2). In addition to the most stable adsorption configuration of each species as seen in Tables 1 and 2, other less stable adsorption configurations are given in Table S1 in the supporting information. We also summarize the previous theoretical calculation results in Table S2 for comparison. As seen from Tables 1, 2 the adsorption energy of CH_4, CH_3, CH_2, O and H increase with the decrease of CN in general, but the most strong adsorption occurred on ad-row (CN=5), instead of ad-atom (CN=3), because both O and CH_2 species prefer to adsorb on two hollow site which ad-atom can not afford due to its limiting active site. For CH_3, it prefers to adsorb on atop site, and the adsorption energy differences are small on all the models. Moreover, in the presence of oxygen species, adsorption energies are generally smaller than those on pure metals due to the competitive adsorption between oxygen atom and CH_x species.

As seen from Table 1 the calculated adsorption energy of methane is very small and the reason is clear that the DFT-GGA calculations usually underestimate the adsorption energy of weakly adsorbed

molecules due to the lack of long-range interaction (i.e. dispersion effect). Indeed, the general correction of dispersion effects to the adsorption energy of aromatic molecules on noble metals is ca. 0.60 eV [56] based on the scheme of Grimme et al.[57,58] To account for the effect of dispersion force on the calculated methane adsorption energy, the dispersion correction was taken into account in this work. Dispersion interactions are empirically defined as the attractive part of the van der Waals-type interaction between atoms and molecules that do not directly bond to each other. Grimme and coworkers have developed efficient methods, DFT-D3 with zero-damping [58] and DFT-D3(BJ) [59] with Becke and Johnson (BJ) damping, [60,61] for the computation of the dispersion interactions in molecules. In this work DFT-D3(BJ) scheme was used to estimate the dispersion force for some typical adsorbed species, where all force field parameters were gained based on the PBE functional as given in ref.[57], which were also applied to DFT calculations with the PW91 functional because both functionals produce very similar total energies. As seen from Table 1, which shows the adsorption energy and dispersion effect correction, the magnitude of the dispersion force is generally in the magnitude within the 0.30 eV or so, smaller than the aromatic molecules.[56] The previous DFT calculation of Henkelman et al. [62] indicated that the adsorption energy of methane on Ir(111) increases by less than 0.10 eV after the correction of dispersion effect.

It is necessary to analyze the adsorption energy trends in terms of bond order conservation principle proposed by Abild-Pedersen et al.[63] for the adsorption energies of any CH_x(x=1~4) species with the adsorption of C atom on transition metal surfaces (so-called 'scaling relationship'). That is $E_{ads}^{CH_x}=\gamma(x)E_{ads}^{C}+\xi$ where E_{ads}^{C} is the adsorption energy of atomic C, $E_{ads}^{CH_x}$ is the adsorption energy of CH_x(x=1~4) species and ξ and γ are the correlation parameters, corresponding to different adsorbates. We give the adsorption properties of carbon atom on various Rh models in Table S3 and the Figure S1 in the supporting information. The DFT results show that the carbon atom adsorption energy varies with the CN of the surface atom, that is, (100)>(211)>ad-atom>(110)>kink >ad-row>(111), and because adsorption site of carbon atom is very complex and strongly depends on the CN of surface metal atom, this trend does not correlate with the CN of surface metal atom. On (100), the adsorption height of carbon atom is very short (ca. 0.20 Å) and nearly parallel to the metal surface, which means it tends to bind more Rh atoms (in fact, the CN of carbon atom is five containing four in the top layer and one in the subsurface layer) and results in the strongest binding energy (-8.06 eV). On ad-atom model, carbon atom inserts into the Rh-Rh bond

and binds to the three Rh atom, leading to a relatively high adsorption energy (-7.82 eV). On (110), carbon atom adsorbed at long bridge site and binds to four Rh metals, i.e. two in the surface layer and two in the subsurface layer, and thus the binding energy is relatively small (-7.79 eV). On ad-row model, carbon atom adsorption energy is smaller (-7.61 eV) because it only binds to two Rh atoms. Due to the fact that the adsorption site of carbon atom strongly depends on the surface topology and the methyl fragment is almost at the top site on all the Rh models investigated in this work, no clear correlation is found for the CH_x species on Rh model catalysts, which differs from the result of previous study about CH_x on the same single crystal face like fcc(111) of a series of transition metals.[54,46]

3.2 Methane dissociation on the clean Rh surfaces

In this section we studied the dissociation of methane and methyl on Rh model catalysts without the pre-adsorbed oxygen species, and the calculated energetic data are summarized in Tables 3 and 4, and Figure 2 displays the optimized IS, TS and TSs. Moreover, we also summarized the previous theoretical calculation results in Table S4 for comparison. The reaction mechanism of methane/methyl dehydrogenation on various Rh models is similar, so we only give the examples of Rh(111), Rh(211) and Rh-ad-atom to describe the methane/methyl dehydrogenation processes. On Rh(111), for the dissociation of methane, the molecular methane adsorbed at the top site at beginning, then close to the adjacent surface metal atom to active its σ-CH bond gradually, and methyl moiety in a little tilted adsorption type. At TS, the formed H species adsorbed between the bridge and hollow sites and the CH_3 fragment adsorbed close to the top site with the distance between abstracted H atom and central carbon atom being 1.55 Å. After TS, methyl diffused to the more stable top site and completed the reaction process. This process undergoes with a barrier of 0.78 eV and endothermic by 0.33 eV. For the dissociation of methyl, the distance between abstracted H atom and central carbon atom was 1.60 Å at TS, and the energy barrier is 0.55 eV and it is exothermic by 0.12 eV. A little difference from other Rh models, there are two successive steps in the dissociation of methane on the stepped Rh(211): In the first step methane approached the step edge Rh atom to form a precursory state for further dehydrogenation, which requires an increase in the energy by 0.10 eV; and in the next step methane dehydrogenated to form methyl, the distance between C and H was 1.53 Å at TS. The calculated energy barrier is 0.61 eV, close to the 0.50 eV reported by Kokalj et al., [40] but larger than the 0.30 eV reported by Liu et al,[9] which is due to the different energy reference used: chemisorbed methane verse gas phase methane. For the dissociation of methyl on Rh(211), it is easily performed with the barrier

of 0.39 eV. At TS, CH_2 species occupied at edge bridge site, and the distance between C and H was 1.70 Å. Clearly, a relatively long distance and thus a weaker competing interaction between H and CH_2 at TS may explain why CH_3 dehydrogenation shows a low barrier. On the ad-atom model, the activation energy of methane dissociation is close to the result reported by Kokalj et al. [40] (0.48 vs 0.46 eV), while the energy barrier of methyl dissociation is a little higher (0.80 vs 0.63 eV).

From Tables 3 and 4 we know that the dehydrogenation barrier decreases with the decrease of CN of the surface atom, agreeing with the general point that the dissociation barrier at defect site is smaller than that of flat one. However, it was found that the barrier is largest on ad-atom (0.80 eV), by enormous contrast with the highest activity of the first dehydrogenation step, and that is because the ad-atom model can not afford sufficient active site to bind the produced CH_2 species which requires at least two active sites. Moreover, it was found that the reaction activation energy of methane dehydrogenation is usually higher than that of methyl dehydrogenation except on ad-atom model, which is in agreement with the reaction energy trend, that is, the produced CH_2 via CH_3 dissociation binds more strongly than that of CH_3 species through CH_4 dissociation in general.

It is necessary to analyze the possible reason why the C-H bond scission barrier varied with the CN of the surface metal atom based on both geometric and electronic effects further. For methane dehydrogenation step, at TSs, the binding energy of H atom does not change with the CN (the energy difference less than 0.13 eV), and the binding energy of CH_3 follows the order of ad-atom (-1.93 eV) > ad-row (-1.83 eV) > (111) (-1.65 eV), in accordance with the CN of surface metal atom, which results in the decreasing in the energy barrier. Moreover, on the more open faces like (100), the two dissociated fragments do not share the same Rh atom as compared to that of (111), and thus give rise to weak repulsive interaction between these two fragments on (100) face, leading to the relatively low energy barrier on the (100) face. [64] In fact, the increased repulsive interaction between the surface species when they bind to the same metal atom is in line with the Bond Order Conservation(BOC) principle proposed by Shustorovich, [65] that is, the valence electrons of the metal atom on the binding shared TS complex would distributed over more bonds than the situation without the shared metal atom, *i.e.,* the clean Rh surfaces.

In addition to the above analysis in terms of the energetic factor, a deep analysis based on the electronic structure was also performed in this work. In general, the catalytic activity of methane dehydrofgenation varies with the coordinate number of surface metal atom, namely the smaller the coordinate number, the stronger is the C-H bond activation. In addition, a linear relation of d-band

center with C-H bond cleavage activation energy is determined on flat surfaces, *i.e.,* the closer the d-band center to the Fermi level, the lower the activation barrier would be.[46,47] Figure 3 shows the relationship between C-H bond cleavage energy barrier and the d-band center of the surface Rh metal for all the models studied in this work. However, the d-band center alone can not explained all the data completely, suggesting that other factor like surface structure may also affect the catalytic activity. For example, as the layer spacing of fcc (110) is relatively shorter compared to those of (111) and (100), and the dissociated H atom can also binds to the subsurface Rh atom at TS, so leading to a low energy barrier for methane dehydorgenation process on Rh(110).

3.3 Methane dissociation on the oxygen pre-adsorbed Rh surfaces

In this section we turned our attention to the methane/methyl dissociation in the presence of oxygen species, and the effect of oxygen species on the activation of C-H bond. Although oxygen atom can act either as reactant in the methane/methyl dissociation directly [$CH_4(CH_3)+O\rightarrow CH_3(CH_2)+OH$], or as "spectator" [$CH_4(CH_3)+O\rightarrow CH_3(CH_2)+H+O$],and here we focused the former case. The ODH of $CH_4(CH_3)+O\rightarrow CH_3(CH_2)+OH$ is in fact a concerted process containing C-H bond breaking and O-H bond formation. The calculation results are given in Tables 3 and 4, and the TSs are shown in Figure 2. The reaction feature is similar on these Rh models, and (111) and ad-atom models are chosen as the examples to describe the whole reaction process. On Rh(111), for the step of $CH_4+O\rightarrow CH_3+H+O$, the oxygen species adsorbed at the fcc site, and the methane molecular adsorbed at the top site of surface Rh atom, with the distance of pre-adsorbed oxygen and stripped hydrogen atom in methane being 2.71 Å. Then molecular methane approached to oxygen atom and the C-H bond was activated gradually. At TS, the CH_3 was nearly located at the top site, and the oxygen atom was located between the top and the fcc sites, and the H was roughly halfway between methyl and oxygen. The distance of C–H/O-H is 1.45/1.21 Å at the TSs. This dissociation process has a barrier of 1.49 eV and it is endothermic by 0.67 eV. For step of $CH_3+O\rightarrow CH_2+OH$, methyl adsorbed at the top site and oxygen remained at the fcc site, and the distance of pre-adsorbed oxygen and stripped hydrogen atom in methyl was 2.50 Å. During the methyl dissociation processes, CH_3 close to the oxygen species and tends to adsorb at the bridge site. At TS, the CH_2 was located nearly at the bridge site, the O atom is located between the bridge and the fcc sites, and the H is roughly halfway between CH_2 and O and far away from the rhodium surface. The distance of C–H/O-H is 1.46/1.36 Å at the TSs. At the FS, both the OH and CH_2 were located at the bridge site. The reaction barrier is 1.15 eV and the corresponding energy change is exothermic by 0.28 eV. On

Rh-ad-atom model, the oxygen species adsorbed at the edge-bridge site, and then methane molecular adsorbed at the top site of surface Rh atom. In such co-adsorption configuration, the distance of pre-adsorbed oxygen and hydrogen in methane is 2.69 Å. This dissociation process has a barrier of 0.75 eV and the dissociation process is exothermic by 0.28 eV. At TS, the CH_3 species binds to the atop site of edge Rh atom with the distance of 2.35 Å, and the distance of C-H/O-H is 1.31/1.41 Å. For the second oxidation step, $CH_3+O \rightarrow CH_2+OH$, the distance of pre-adsorbed oxygen and hydrogen in methane is 3.21 Å. This dissociation process has a barrier of 0.76 eV and it is endothermic by 0.18 eV. At TS, the distance of C-H/O-H is 1.44/1.21 Å.

Based on above calculation results we find that the C-H bond length in TSs is general smaller than that on clean Rh surfaces due to the interaction between O_{ad} and H species at TSs. It is found that when the Rh surface is modified by the chemisorbed oxygen species, its dehydrogenation behave dramatically changes. In general, the chemisorbed oxygen species increases the value of barriers in most surfaces of Rh in this study, indicated the poison effect of oxygen atom in the processes of methane dissociation. This result is consistent with our previous study as well as the experimental observations that the X-H bond activation is usually hinted by the chemisorbed oxygen on more active metals like Rh. However, on the ad-atom model, the catalytic activity of methyl dissociation is even higher on oxygen pre-adsorbed system than that on clean one, which means that the process of methane partial oxidation may be comparable to that of methane dissociation on the Rd-ad-atom model catalysts.

It should be pointed that the effect of dispersion force on the activation energy is very complex because the dispersion force not only affects the reactant but also affects the transition state, and the exactly activation energy calculation should be taken by considering the dispersion force for both the reactant and transition state. Tables 3 and 4 give the calculated results for the effect of dispersion force on the energy barrier based on the DFT-D3 method.[57] As seen from Tables 3 and 4 we can know that the dispersion force correction has a relative large effect on the methane dehydrogenation reaction, and has a little effect on the methyl dehydrogenation step. The reason is apparently because the effect of dispersion force correction is large on the methane due to this physisorption character, whereas it is little on the methyl because of its chemisorption character. Interestingly, we find that the barrier of methyl dehydrogention in the presence of oxygen atom is smaller than that of the direct dehydrogenation after the dispersion force correction(0.66 verse 0.77 eV). It must be pointed out that the activation energy barrier corrected by DFT-D3 method is usually smaller than that of standard

DFT-GGA method (see Tables 3 and 4), whereas the more accurate calculation based on the van der Waals density functional (vdW-DF) [66,67] indicated that the activation barrier is large than the standard DFT-GGA calculation (0.98 eV for methane dehydrogenation on Rh(111)).The detailed discussion of dispersion force correction on the activation energy will be given in our future work.

3.4 The general rule of oxygen species in the activation of C-H bond

Based on above calculation results, it can be seen qualitatively that the more strongly the oxygen atoms adsorb on the surface, the smaller the promoting effect would be. The possible reason is that the pre-adsorbed atomic oxygen occupies the high-symmetry site, which can interact with both metal atoms and reactant molecule, where competition exists. So if the atomic oxygen strongly binds to the metal surface, a weak interaction will form between it and the breaking H atom, and presents a less promoting effect. To confirm such point, the correlation between energy barrier change ($\Delta E_a = E_{a1} - E_{a2}$, where E_{a1} and E_{a2} are the reaction barriers with and without atomic oxygen respectively) and the binding energy of atomic oxygen ($E_{ads}(O)$) was investigated, and the fitting linear correlation is shown in Figure 4. For all 28 reactions involved in this work, a roughly linear correlation was found between barrier difference and oxygen adsorption energy except methyl dissociation on ad-atom model. The linear correlation was strong for the methane step, but less strong for the methyl dissociation, for which the reason is clear that the CH_3 fragment always stays at the top site in the methane dissociation, but the CH_2 fragment via the methyl dissociation stays depending on the surface geometry of Rh surface.

It is worthy to analyze the reason behind the oxygen activation for methane dissociation. Here two methods were applied in the following analysis.

a) Energy barrier decomposition scheme analysis

For dissociation reactions like $AB \rightarrow A+B$, the adsorption energy of $A+B$ activated complex at the TS can be divided into three parts: $E_{A+B}^{TS} = E_A^{TS} + E_B^{TS} + E_{Int}^{TS} = \Sigma^{TS} + E_{Int}^{TS}$,[31] here $E_A^{TS}(E_B^{TS})$ is the adsorption energy of reactant A(B) at TS without B(A), and E_{int}^{TS} is the interaction energy between A and B at TS. And therefore the dissociation barrier can be written as $E_a = \Sigma^{TS} + E_{Int}^{TS} - E_{AB}^{IS} - E_{AB}^{(g)}$, where E_{AB}^{IS} is the adsorption energy of AB at IS, and $E_{AB}^{(g)}$ is the bond energy of AB at gas phase which was calculated by the equation E_{AB}-E_A-E_B. Table 5 gives the calculated barrier decomposition results of methyl dissociation on (111), ad-row and ad-atom with and without the oxygen species. For

methyl dehydrogenation, $E_{AB}^{(g)}$ is calculated to be -5.04 eV. On these three models the presence of oxygen species weakens the adsorption energy of A(B) at TS but increases the interaction between A and B at TS, both of which lead to the increase of the barrier of methyl dissociation. Due to the similarity between (111) and ad-row, we only give a detailed analysis of ad-row and ad-atom models. On ad-row model, at TS, the CH_2 fragment adsorbed on the edge-bridge site with the average bond distance of $d_{C\text{-}Rh}$ was 2.05 Å, and the H fragment adsorbed on the edge-top site with the adsorption height of 1.62 Å. In the presence of oxygen species, at TS, the CH_2 fragment in a tilted edge-top site with the $d_{C\text{-}Rh}$ of 2.11 Å, and the H fragment in a edge-top site with the adsorption height of 1.86 Å. Obviously, being far away from the substrate weakens the adsorption strength of both CH_2 and H fragments in the presence of oxygen species. For the interaction part, we find this magnitude even becomes an attractive interaction in the presence of oxygen atom as compared to the situation without oxygen species, which would reduce the reaction barrier to some extent. For the magnitude of E_{Int}^{TS}, it can be considered as the contributions of direct Pauli repulsion, bonding competition and electrostatic interaction between H and CH_2 in the TS configuration. Since the distances between H and CH_2 at TS configuration are usually smaller when oxygen atom exists(see Tables 3 and 4), and also considering that the fragments of CH_2 and H at TS shared one surface Rh atom in spit with and without oxygen atom, one may believe that the change in the E_{Int}^{TS} is mainly due to the electrostatic interaction. For the magnitude of electrostatic interaction, it was roughly estimated from sign of charge of central C atom and H atom, which can be analyzed by Bader charge scheme (see Table 6). Fortunately, the Bader charge analysis shows that the charge sign of C is always negative and the H atom changed from negative to positive due to the strong electron withdraw of O atom.

On ad-atom model, in the presence of oxygen species, both the CH_2 fragment and H fragment were far away from Rh surface, which means a very weak adsorption of CH_2 and H at the TS geometry, and more energy would be cost when CH_2/H moves from IS to TS than that of clean one, and thus increases the reaction barrier to some extent. However, the attractive interaction between CH_2 and H on the O/ad-atom system is far more stronger than that on clean model due to the strong electrostatic interaction according to the Bader charge analysis results as seen in Table 6. And the combination of above two opposite parts makes the reaction barrier of methyl dissociation changed a little on the oxygen pre-adsorbed Rh-ad-atom model.

It is important to analyze the reason why TS is destabilized by the oxygen atom. Firstly, oxygen atom causes the change of d-band center may be one of the possible reason. In the presence of oxygen atom, the d-band center of surface Rh metal atom generally away from the Fermi level, indicated the less active of metallic atom. The reason is clear because of the large electronegative of oxygen atom and withdraw electrons from Rh atom. So the binding energy of CH_2+H at TS would become less stable in the form of oxygen-preadsorbed Rh surfaces, which leading to the high activation energy barrier. This can also be confirmed based on the feature of TS complex. For the methyl dehydrogenation on pure Rh(111), both CH_2 and H species binds to the Rh atoms and with relatively strong binding energy; In the presence of oxygen atom, however, both CH_2 and H species are far away from the Rh surface due to the existence of oxygen atom, and thus leading to the weak interaction between TS complex and substrate. Secondly, by analyze the TSs carefully we find that the TS complex in the presence of oxygen atom shows a CH_2--H--O feature, in which C, H and O atoms shared with same Rh atom. From the point of BOC,[65] the valence electrons of the metal Rh atom at the TS complex would become more distributed compared to the case of direct dehydrogenation on Rh(111), and thus results in a weak interaction with the TS complex.

b) Acid-Base pair interaction model analysis

For the effect of chemisorbed O_{ad} on the methane dissociation on Rh surfaces, the Rh atom may act as Lewis acid site and O_{ad} atom may act as Brønsted base site for the proton abstraction from methane/methyl, and the acid-base sites interact with molecular methane/methyl simultaneously, which lead to the higher activity in the methane dissociation (see Figure 4). [68-70] The magnitude of acid and base was measured by the electron charge change based on the Bader charge analysis, that is, the Lewis acid is an electron acceptor and the Lewis base is an electron donor. Apparently, positively charged on Rh atom and negatively charged in O species means a strong Acid-Base interaction and would result in strong promoting in the activation of C-H bond. Similarly, the methyl dehydrogenation on (111), ad-row and ad-atom are chosen in such kind of analysis. The Bader charge analysis results show that the Bader valence (BV) is +0.22 *e* on Rh atom and -0.77 *e* on O_{ad} on (111), +0.36 e on Rh atom and -0.73 e on O_{ad} on add-row, and +0.62 e on Rh atom and -0.60 e on O_{ad} on ad-atom . Clearly, the trend of BV difference between Rh and O_{ad} is ad-atom (1.22 e) > ad-row (1.09 e) > (111) (0.99 e), is consistent with the barrier trend as seen in Table 4, namely 0.76 eV for ad-atom model, 0.88 eV for ad-row model and 1.15 eV for (111) model. It should be pointed out that the H-CHx bond cleavage in methane/methyl is in fact a heterlytic bond cleavage processes over the oxygen-preadsorbed Rh

surfaces, that is, CHx species adsorbed on the metal Rh site, and the dissociated H atom binds to the oxygen atom to form OH species. The previous DFT study of Li et al. indicated that the C-H bond cleavage energy barrier is correlated well with the acid strength of oxygen atom, namely the weaker acid of oxygen atom related to the higher activity in the C-H bond cleavage.[71] Clearly, this is consistent with our present results: the strong binding energy of oxygen atom means weak acid strength and thus a high re-activity in the C-H bond activation.

4. Conclusions

The present calculation results show that the adsorption energy of CH_X does not linearly correlate with the carbon atom adsorption energy due to the different adsorption site of CH_x on the Rh model catalysts. The reaction path study indicates that the pre-adsorbed oxygen atom significantly inhibits the methane dehydrogenation on Rh surface, whereas it shows very little effect or even become promotion effect on the methyl dehydrogenation step on ad-atom model, which means that the O_{ad} may act as a active site. Moreover, the possible physical nature behind the oxygen effect has been analyzed by the barrier decomposition method, and it was found that the presence of oxygen atom reduces the adsorption energy of dissociated fragments but increases the interaction between the dissociated fragments, and the whole result increases the reaction barrier.

ACKNOWLEDGEMENTS

This work was supported by the State Key Program of Natural Science of Tianjin (Grant No. 13JCZDJC26800), MOE Innovation Team (IRT13022) of China, NSFC(21421001), the State Key Program of National Natural Science Foundation of China(Grant No. 21433008), and the foundation of State Key Laboratory of Coal Conversion (Grant No. J15-16-908).

References

1 G. A. Somorjai, *Surface Chemistry and Catalysis* (Wiley, New York, 1994).

2 G. A. Somorjai, *J. Mol. Struct. (THEOCHEM)* 1998, **424**, 101.

3 R. F. Hicks, H. Qi, M. L. Young,R. G. Lee, *J. Catal*.,1990, **122**, 280-294.

4 J. R. Engstromf, D. W. Goodman, and W. H. Weinberg, *J. Am. Chem. Soc.,* 1986, **108***,* 4653-4655;

5 R. J . Madix, Acc. Chem. Res., 1979, **12**, 265-270.

6 J.T. Yates Jr., *J. Vac. Sci. Technol. A*, 1995, **13,** 1359-1367.

7 T. Zambelli, J. Wintterlinn, J. Trost and G. Ertl, *Science, 1996,* **273**, 1688-1690.

8 S. Dahl, A. Logadottir, R. C. Egeberg, J. H. Larsen, I. Chorkendorff, E. Tornqvist and J. K. Norskov, *Phys. Rev. Lett.*,1999, **83**, 1814-1817.

9 Z. P. Liu and P. Hu, *J. Am. Chem. Soc*., 2003, **125,** 1958-1967.

10 I. M. Ciobîcã and R. A. van Santen, *J. Phys. Chem. B,* 2004, **107,** 3808-3812.

11 R.T. Vang, K. Honkala, S. Dahl, E. K. Vestergaard, J. Schnadt, E. Lgsgaard, B. S. Clausen, J. K. Norskov and F. Besenbacher, *Nature materials,* 2005, **4**,160-162.

12 T. P. Beebe Jr., D. W. Goodman, B. D. Kay and J. T. Jr. Yates, *J. Chem. Phys*., 1987, **87,** 2305.

13 I. Chorkendorff, I. Alstrup and S. Ullmann, *Surf. Sci*., 1990, **227**, 291-296.

14 H. S. Bengaard, I. Alstrup, I. Chorkendorff, S. Ullmann, J. R. Rostrup-Nielsen and J. K. Norskov, *J. Catal*. 1999, **187**, 238-244.

15 R. D. Beck, P. Maroni, D. C. Papageorgopoulos, T. T. Dang, M. P. Schmid and T. R. Rizzo, *Science*, 2003, **302**, 98-100.

16 J. Wei and E. Iglesia, *J. Catal*., 2004, **225**, 116-127.

17 R. Horn, K. A. Williams, N. J. Degenstein, A. Bitsch-Larsen, D. Dalle Nogare, S. A. Tupy and L. D. Schmidt, *J. Catal.,* 2007, **249**, 380-393.

18 M. A. Quinlan, B. J. Wood and H. Wise, *Chem. Phys. Lett*., 1985,**118**, 478-480.

19 M. Valden, N. Xiang, J. Pere and M. Pessa, *Appl. Surf. Sci*., 1996, **99**, 83-89.

20 M. P. Schmid, P. Maroni, R. D. Beck, and T. R. Rizzo, *J. Chem. Phys.*, 2002, **117**, 8603.

21 C. T. Au, C. F. Ng and M. S. Liao, *J. Catal.*, 1999**,185**, 12-22.

22 B. Xing, X. Y. Pang, G. C. Wang and Z. F. Shang, *J. Mol. Catal. A: Chem.*, 2010, **315**, 187-196.

23 V. A. Kondratenko, C. Berger-Karin and E. V. Kondratenko, *ACS Catal*., 2014, **4**, 3136-3144.

24 A. Beretta, A. Donazzi, G. Groppi, M. Maestri, E. Tronconi and P. Forzatti, *Catalysis*, 2013,**25**, 1-49

25 P. W. van Grootel, E. J. M. Hensen and R. A. van Santen, *Langmuir*, 2010, **26**, 16339-16348.

26 T. Zhu, P. W. van Grootel, Ivo A. W. F., S. Sun, R. A. van Santen and E. J.M. Hensen, *J. Catal.*, 2013, **297**, 227-235.

27 D. Pakhare and J. Spivey, *Chem. Soc. Rev*., 2014, **43**, 7813-7837.

28 B. S. Bunnik and G. J. Kramer, *J. Catal.*, 2006, **242**, 309-318.

29 E. J. Walter and A. M. Rappe, *Surf. Sci*.,2004,**549**, 265-272.

30 A. Kokalj, N. Bonini, C. Sbraccia, S. De Gironcoli and S. Baroni, *J. Am.Chem. Soc*., 2004,**126,** 16732-16733.

31 G. Fratesi and S. de Gironcoli, *J. Chem. Phys*., 2006, **125**, 044701.

32 B. Wang, L. Song, and R. Zhang, *Appl. Surf. Sci.*, 2012, **258**, 3714-3722.

33 P. W. Van Grootel, R. A. Van Santen, and E. J. M. Hensen, *J. Phys. Chem.C,* 2011, **115**, 13027-13034.

34 A. Trinchero, A. Hellman, and H. Grönbeck, *Surf. Sci.*, 2013, **616**, 206-213.

35 Y.-H. Chin, C. Buda , M. Neurock, and E. Iglesia, *J. Catal.,*2011, **283**, 10-24.

36 Y. Chen and D. G. Vlachos, *Ind. Eng. Chem. Res*., 2012, **51**, 12244-12252.

37 F. Vines, Y. Lykhach, T. Staudt, M.P. A. Lorenz, C. Papp, H. P. Steinruck, J. Libuda, K.M. Neyman and A. Gorling, *Chem. Eur. J.*, 2010, **16**, 6530-6539.

38 C. J. Zhang and P. Hu, *J. Chem. Phys*., 2002, **116**, 4281.

39 W. Tang, Z. Hu, M. Wang, G. D. Stucky, H. Metiu and E. W. McFarland, *J. Catal*., 2010,**273**, 125-137.

40 D. Mei, V.-A. Glezakou, V. Lebarbier, L. Kovarik, H. Wan, K. O. Albrecht, M. Gerber, R. Rousseau and R. A. Dagle, *J. Catal*., 2014, **316**, 11-23.

41 X.-F. Yang, A. Wang, B. Qiao, J. Li , J. Liu and T. Zhang, *Acc. Chem. Res.*, 2013, **46**, 1740-1748.

42 P. A. Thiel and T. E. Madey, *Surf. Sci. Rep*., 1987, **7**, 211-385.

43 E. Shustorovich and A. T. Bell, *Surf. Sci.,* 1992, **268**, 397-405.

44 G.-C. Wang, S.-X. Tao and X.-H. Bu, *J. Catal*., 2006, **244**, 10-16.

45 C.-Q. Lv, K.-C. Ling and G.-C. Wang, *J. Chem. Phys.*, 2009,**131**, 144704.

46 B. Xing, X.-Y. Pang and G.-C. Wang, *J. Catal.*, 2011, **282**, 74-82.

47 B. Xing, and G.-C. Wang, *Phys. Chem. Chem. Phys***., 2014,16,** 2621-2629.

48 G. Kresse and J. Hafner, *Phys Rev B*.,1993,**47,** 558-561.

49 G. Kresse and J. Furthmüller, *Comp. Mater. Sci*., 1996, **6**, 15-60.

50 G. Kresse and J. Furthmüller, *Phys. Rev. B*, 1996, **54**, 11169-11186.

51 P. Perdew and Y. Wang, *Phys. Rev. B*,1992, **45**, 13244-13249.

52 P. E. Blöchl, *Phys. Rev. B*, 1994, **50**, 17953-17979.

53 G. Kresse and D. Joubert, *Phys. Rev. B*, 1999, **59**, 1758-1775.

54 H. J. Monkhorst and J. D. Pack, *Phys. Rev. B*, 1976, **13**, 5188-5192.

55 G. Mills and H. Jonsson, *Phys. Rev. Lett*., 1994, **72**, 1124-1127.

56 K. Tonigold and A. Gross, *J. Chem. Phys.*, 2010, **132**, 224701.

57 S. Grimme, *J. Comput. Chem.*, 2006, **27**, 1787-1799.

58 S. Grimme, J. Antony, S. Ehrlich and H. Krieg, *J. Chem. Phys*., 2010, **132**, 154104.

59 S. Grimme, S. Ehrlich and L. Goerigk, *J. Comput. Chem.*, 2011, **32**, 1456-1465.

60 A. D. Becke and E. R. Johnson, *J. Chem. Phys*., 2005, **122**, 154104-154105.

61 E. R. Johnson and A. D. Becke, *J. Chem. Phys.,* 2006, **124**, 174104.

62 G. Henkelman and H. Jónsson, *Phys. Rev. Lett*., 2001, **86,** 664-667.

63 F. Abild-Pedersen, J. Greeley, F. Studt, J. Rossmeisl, T. R. Munter, P. G. Moses, E. Skúlason, T. Bligaard and J. K. Nørskov, *Phys. Rev. Lett*., 2007, **99**, 016105.

64 R. A. Van Santen,W.K.Offermans, J.M.Ricart, G.Novell-Leruth and J.Perez-Ramirez, *J.Phys:Conference series,* 2008, **117**,012028.

65 E. Shustrovichm, *Surf. Sci. Rep.*, 1986, **6**,1

66 M. Dion, H. Rydberg, E. Schr¨oder, D. C. Langreth, and B. I. Lundqvist, Phys. Rev. Lett. **92**, 246401 (2004).

67 J. Klime˘s, D. R. Bowler, and A. Michaelides, *Phys. Rev. B* 2011, **83**, 195131.

68 S. G. Podkolzin, O. V. Manoilova, and B. M. Weckhuysen, *J. Phys. Chem.* B, 2005, **109**, 11634-11642.

69 K. Shimizu, T. Kubo, A. Satsuma, T. Kamachi and K. Yoshizawa, *ACS Catal*., 2012. **2**, 2467-2474.

70 Y.Q. Wang, L.F.Yan and G.-C.Wang, *Phys. Chem. Chem. Phys*., 2015, **17**, 8231-8238.

71 H.Y. Li, Y. L. Guo, Y. Guo, G. Z. Lu and P. Hu, *J.Chem. Phys.*, 2008, **128**, 051101.

Figure captions:

Figure 1 Adsorption sites of Rh(hkl) surfaces.

Figure 2 DFT optimized IS, TS and FS of methane/methyl dehydrogenation on clean and oxygen pre-adsorbed Rh models

Figure 3 Methane dehydrogenation barrier verse d-band center

Figure 4 Relationship between barrier difference with and without oxygen species and the adsorption energy of oxygen atom on various Rh model catalysts. a) Both methane and methyl dissociation, b) methane dissociation..

Figure 5 Schematic for for methane dissociation process via the Acid-base interaction model.

Table 1 Adsorption energy of methane on various Rh-model catalysts (eV)

	111	100	110	211	Kink	Ad-row	Ad-atom
DFT	-0.03	0.04	-0.04	-0.16	-0.05	-0.08	-0.09
DFT-D3(PBE)	-0.38	-0.16	-0.15	-0.26	-0.13	-0.16	-0.11

Table 2 Adsorption energies and geometry parameters of O, H, CH_3 and CH_2 on Rh surfaces

	O		H		CH_3		CH_2	
	Site	E_{ads}(eV)	Site	E_{ads}(eV)	Site	E_{ads}(eV)	Site	E_{ads}(eV)
(111)	FCC	-5.14	FCC	-2.82	Top	-1.84	FCC	-4.12
(100)	4h	-5.24	4h	-2.72	Top	-2.01	4h	-4.51
(110)	Sb	-5.32	Sb	-2.70	Top	-2.21	Sb	-4.58
(211)	EB	-5.43	EB	-2.87	Top	-2.35	EB	-4.58
Kink	K3H	-5.18	K3H	-2.84	Top	-2.24	KB	-4.64
Ad-row	EB	-5.69	EB	-2.88	Top	-2.42	EB	-4.68
Ad-atom	EB	-4.80	EB	-2.87	Top	-2.25	EB	-4.52

Note: EB means Edge-bridge, KB mean Kink-bridge, K3H means Kink-3H and E3H means the Edge-3H.

Table 3 Energetic and distances at the TSs of methane dissociation on Rh models

	Clean surface			O/Rh surface			
Surfaces	E_a(eV)	ΔH(eV)	C-H(Å)	E_a(eV)	ΔH(eV)	C-H(Å)	O-H(Å)
111	0.78 (0.62)	0.33 (0.11)	1.55	1.49 (1.36)	0.67 (0.50)	1.45	1.21
100	0.65	0.23	1.55	1.30	0.56	1.48	1.22
110	0.51	0.02	1.61	0.84	-0.32	1.54	1.69
211	0.61	-0.07	1.53	1.46	0.09	1.38	1.23
Kink	0.65	0.13	1.61	1.30	-0.13	1.45	1.20
Ad-row	0.54 (0.40)	-0.21 (-0.38)	1.63	1.45 (1.36)	0.08 (-0.23)	1.43	1.21
Ad-atom	0.42 (0.31)	0.01 (-0.11)	1.63	0.75 (0.69)	-0.28 (-0.42)	1.31	1.41

Note: The date in parenthesis are the calculation reulst based on the DFT-D3 method.

Table 4 Energetics and distances at the TSs of methyl dissociation on Rh models

	Clean surface			O/Rh surface			
Surfaces	E_a(eV)	ΔH(eV)	C-H(Å)	E_a(eV)	ΔH(eV)	C-H(Å)	O-H(Å)
111	0.55 (0.52)	-0.12 (-0.18)	1.60	1.15 (1.16)	0.28 (0.32)	1.46	1.36
100	0.28	-0.12	1.68	0.47	-0.05	1.47	1.34
110	0.36	-0.06	1.57	0.90	0.43	1.22	1.47
211	0.39	-0.13	1.70	1.15	0.35	1.47	1.33
Kink	0.53	0.31	1.79	1.32	0.03	1.48	1.33
Ad-row	0.38 (0.37)	-0.24 (-0.26)	1.66	0.88 (0.88)	-0.50 (-0.50)	1.42	1.30
Ad-atom	0.80 (0.77)	0.10 (0.02)	1.63	0.76 (0.66)	0.18 (0.00)	1.44	1.21

Note: The date in parenthesis are the calculation reulst based on the DFT-D3 method.

Table 5 Energy decomposition of the calculated activation energy of methyl dissociation (eV).

	Rh				O/Rh			
	E_a	ΣE^{TS}	E_{Int}^{TS}	E_{AB}^{IS}	E_a	ΣE^{TS}	E_{Int}^{TS}	E_{AB}^{IS}
(111)	0.38	-6.40	-0.09	-1.84	1.15	-5.00	-0.73	-1.84
Ad-row	0.38	-7.08	0.00	-2.42	0.88	-5.05	-0.85	-1.74
Ad-atom	0.80	-6.45	-0.04	-2.25	0.83	-1.10	-5.60	-2.49

Table 6 Bader charge analysis of TS for methyl dissociation with and without oxygen atom

	Rh		O/Rh	
	$C(H_2)$ /*e*	H /*e*	$C(H_2)$ /*e*	H /*e*
(111)	-0.35	-0.08	-0.28	0.30
Ad-row	-0.36	-0.12	-0.23	0.31
Ad-atom	-0.27	-0.12	-0.31	0.38

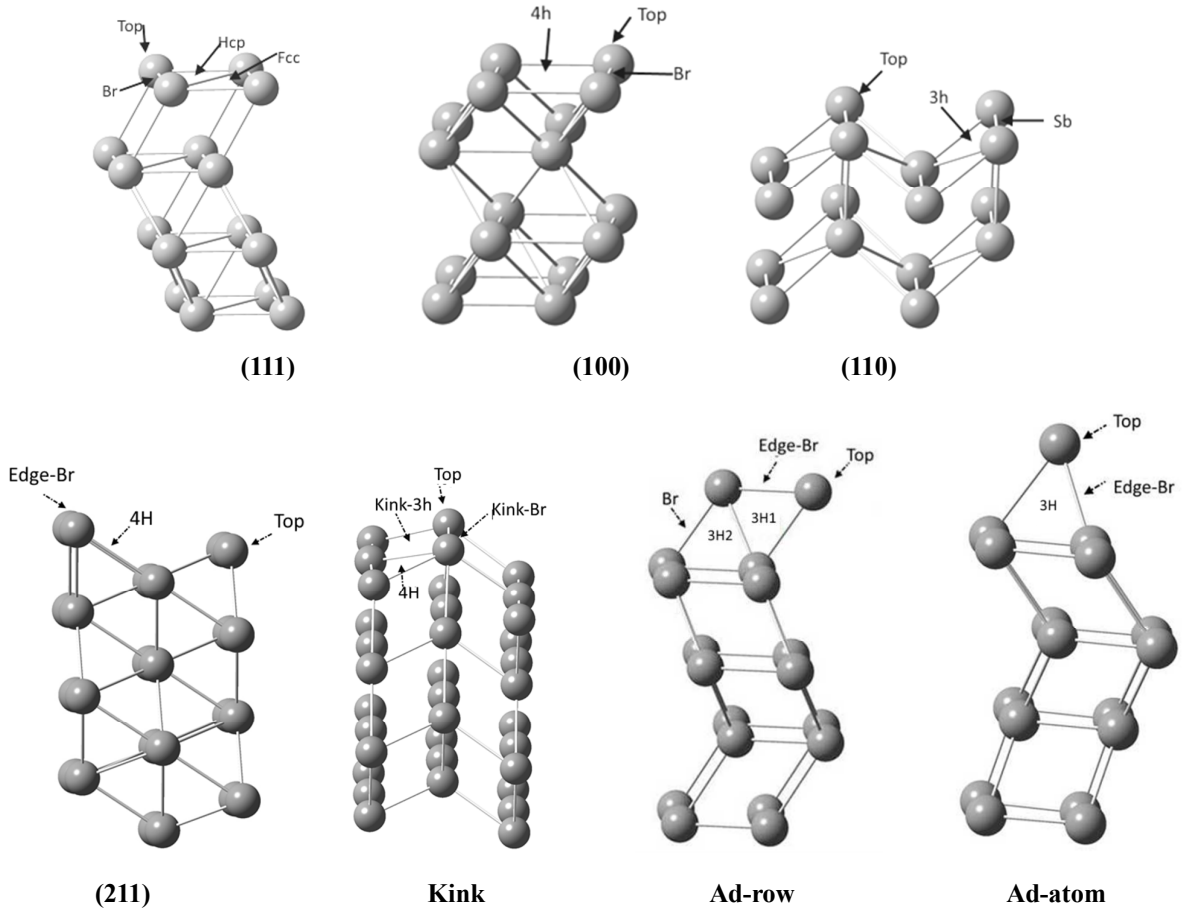

Figure 1

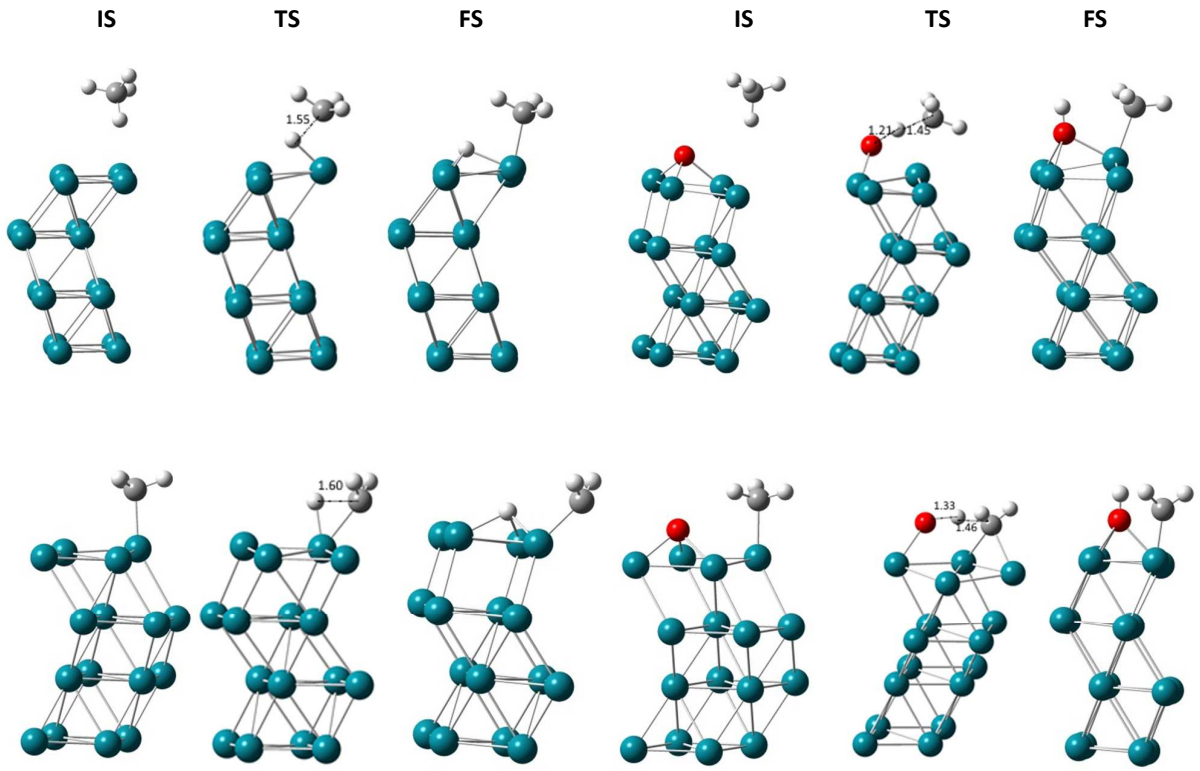

(111)

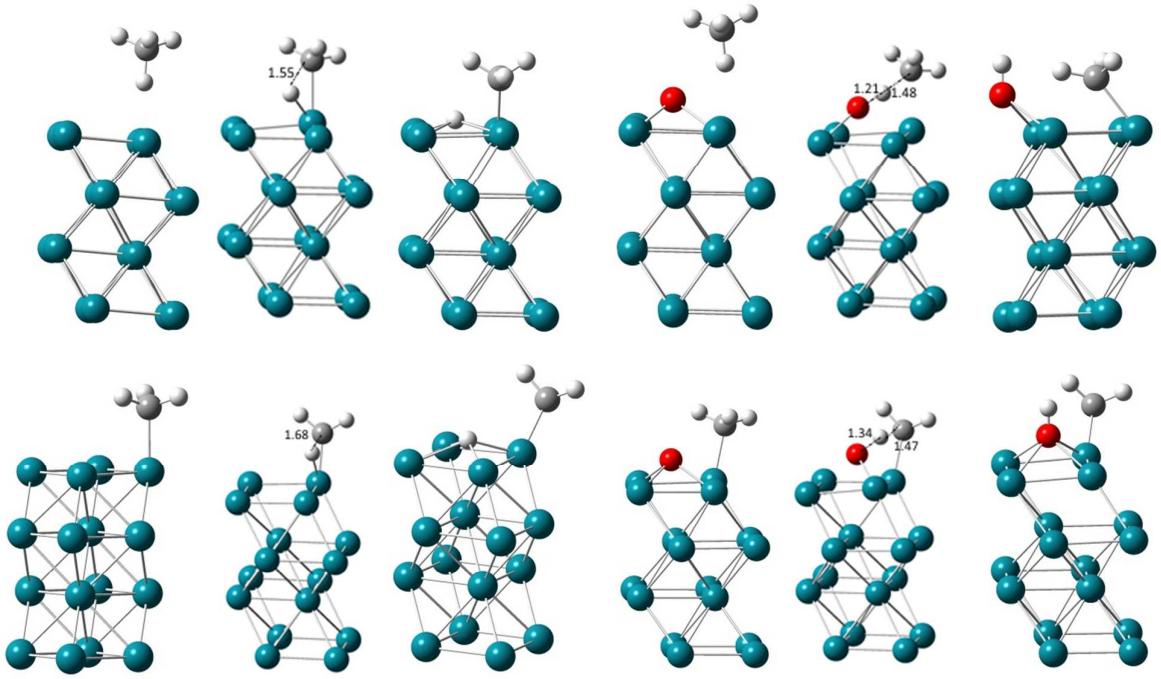

(100)

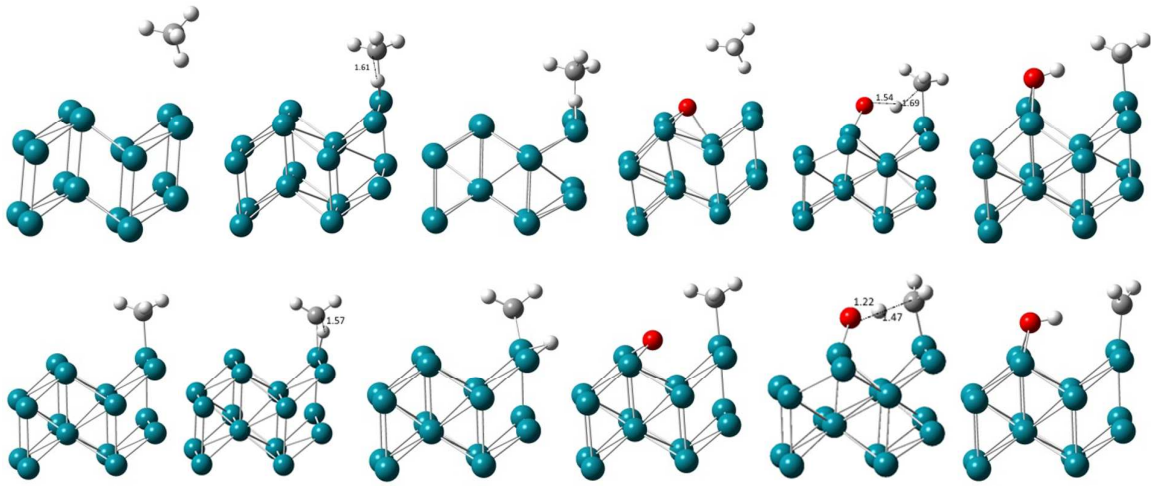

(110)

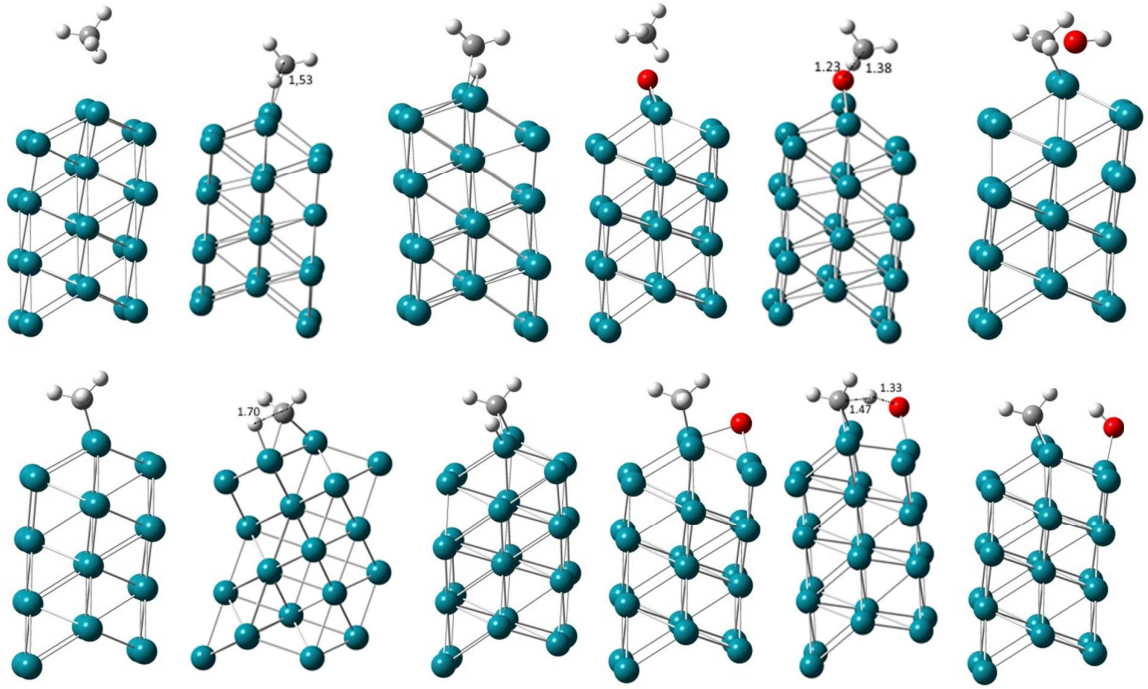

(211)

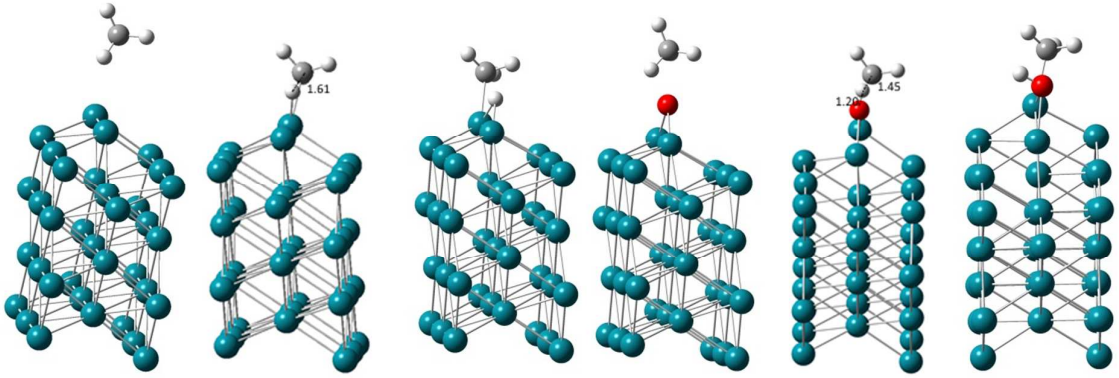

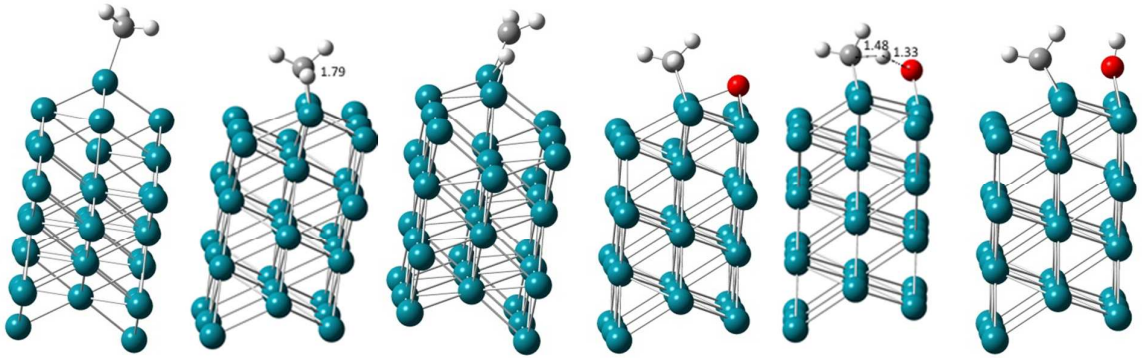

Kink

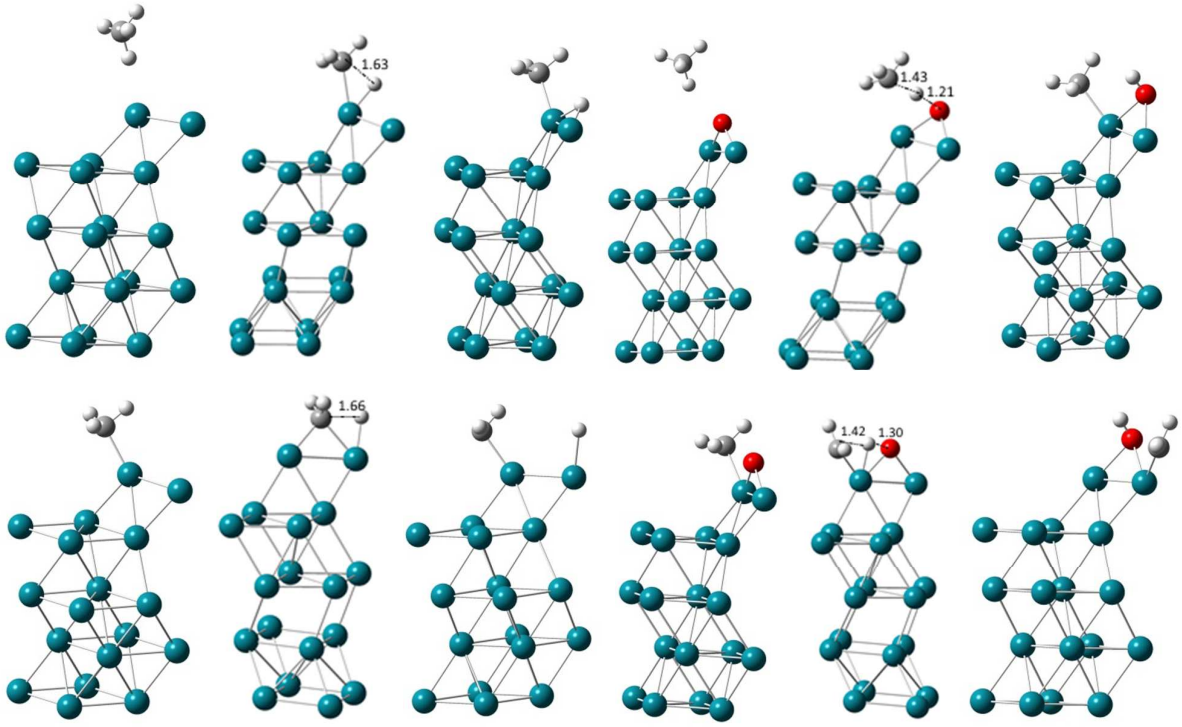

Ad-row

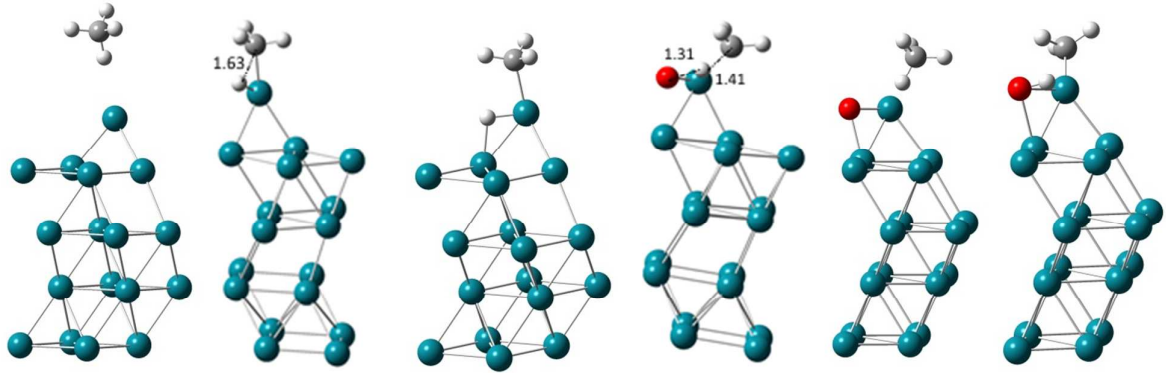

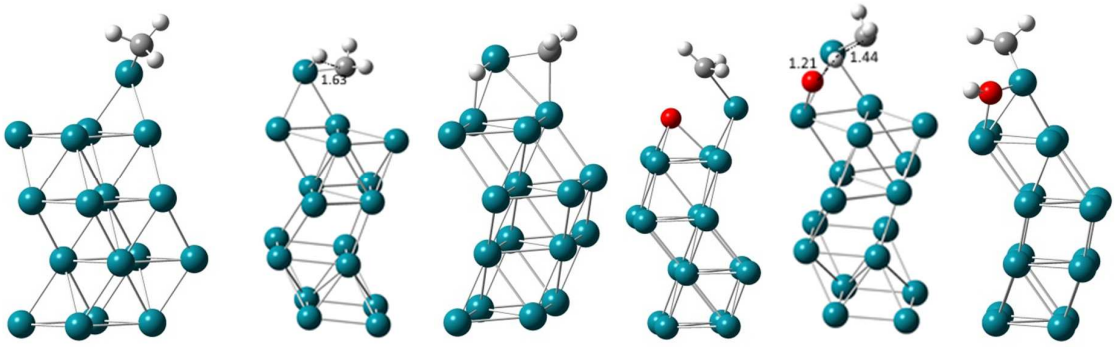

Ad-atom

Figure 2

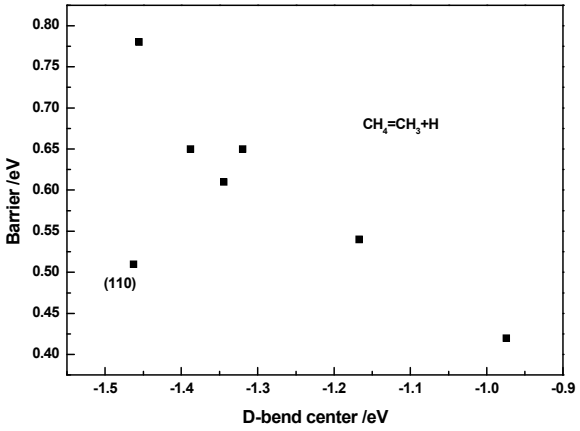

Figure 3

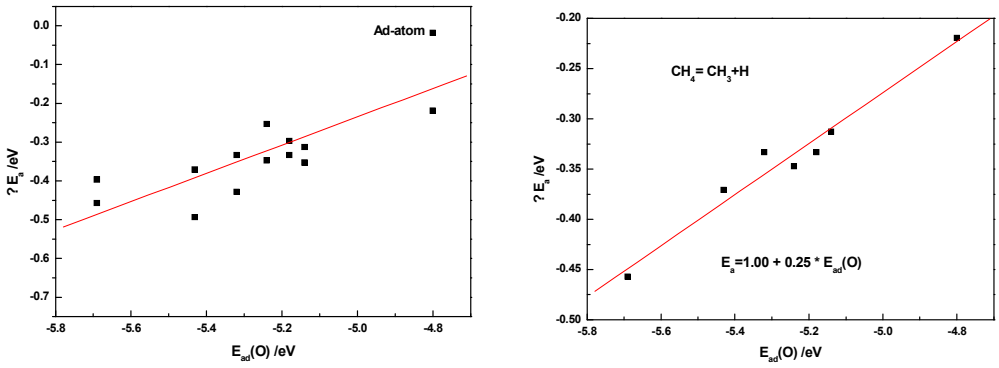

a) b)

Figure 4

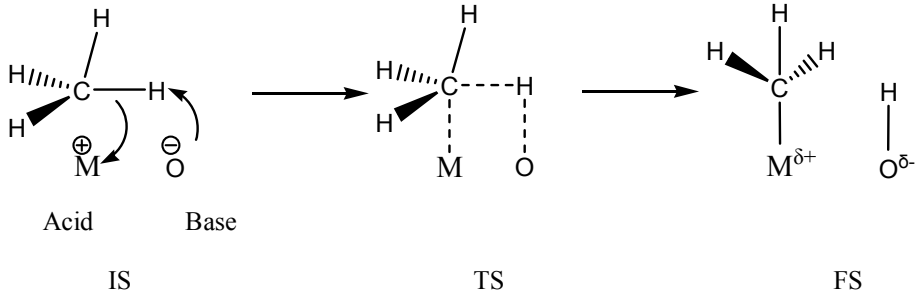

Figure 5